NEOPLASIA
www.neoplasia.com

Volume 17 Number 3 March 2015 pp. 265–278 265

# ABCG2 Localizes to the Nucleus and Modulates *CDH1* Expression in Lung Cancer Cells[1,2,3]

**Shu-Ching Liang[*,4], Chih-Yung Yang[†,4], Ju-Yu Tseng[*], Hong-Ling Wang[‡], Chien-Yi Tung[*], Hong-Wen Liu[*], Chin-Yau Chen[§], Yi-Chen Yeh[¶], Teh-Ying Chou[‡,¶,#], Muh-Hwa Yang[#,**], Jacqueline Whang-Peng[††,‡‡] and Chi-Hung Lin[*,§§]**

*Institute of Microbiology and Immunology, National Yang-Ming University, Taipei, Taiwan; [†]Department of Education and Research, Taipei City Hospital, Taipei, Taiwan; [‡]Institute of Biochemistry and Molecular Biology, National Yang-Ming University, Taipei, Taiwan; [§]Department of Surgery, National Yang-Ming University Hospital, Yilan, Taiwan; [¶]Department of Pathology and Laboratory Medicine, Taipei Veterans General Hospital, Taipei, Taiwan; [#]Institute of Clinical Medicine, National Yang-Ming University, Taipei, Taiwan; [**]Division of Hematology-Oncology, Department of Medicine, Taipei Veterans General Hospital, Taipei, Taiwan; [††]Division of Cancer Center, Wan Fang Hospital, Taipei Medical University, Taipei, Taiwan; [‡‡]Center of Excellence for Cancer Research, Taipei Medical University, Taipei, Taiwan; [§§]Institute of Biophotonics, National Yang-Ming University, Taipei, Taiwan

## Abstract

Breast cancer resistance protein [BCRP/ATP-binding cassette subfamily G member 2 (ABCG2)] is a member of the ATP-binding cassette transporter family. The presence of ABCG2 on the plasma membrane in many kinds of human cancer cells contributes to multidrug resistance during chemotherapy, and it has been used as the side population marker for identifying cancer stem cells in lung cancers. We report here that, in addition to the membranous form, ABCG2 proteins are also found inside the nucleus, where they bind to the E-box of *CDH1* (E-cadherin) promoter and regulate transcription of this gene. Increased expression of *ABCG2* causes an increase of E-cadherin and attenuates cell migration, whereas knockdown of *ABCG2* downregulates E-cadherin and enhances cell motility. In mice, xenografted A549 cells that have less ABCG2 are more likely to metastasize from the subcutaneous inoculation site to the internal organs. However, for the cancer cells that have already entered the blood circulation, an increased level of ABCG2, and correspondingly increased E-cadherin, may facilitate circulating cancer cells to colonize at a distant site and form a metastatic tumor. We propose a novel role for nuclear ABCG2 that functions as a transcription regulator and participates in modulation of cancer metastasis.

*Neoplasia (2015) 17, 265–278*

Abbreviations: ABCG2, ATP-binding cassette subfamily G member 2; CDH1, E-cadherin; ChIP, chromatin immunoprecipitation; CSC, cancer stem cell; EMT, epithelial-mesenchymal transition; EMSA, electrophoretic mobility shift assay; MET, mesenchymal-epithelial transition; NLS, nuclear localization signal; SP, side population

Address all correspondence to: Jacqueline Whang-Peng, MD, Division of Cancer Center, Municipal Wan Fang Hospital, Taipei Medical University, No. 111, Sec. 3, Hsing-Long Rd, Taipei 11696, Taiwan; Chi-Hung Lin, MD, PhD, Institute of Microbiology and Immunology, National Yang-Ming University, No. 155, Sec. 2, Linong Street, Taipei 11221, Taiwan.
E-mail: jqwpeng@nhri.org.tw

[1] Grant support: This work was supported by the National Science Council (NSC103-2319-B-010-001 and NSC 102-2325-B-010-013) to C.-H.L. and by a grant from the Ministry of Education, Aim for the Top University Plan in Taiwan.
[2] Conflicts of interest: No potential conflicts of interest were disclosed.
[3] This article refers to supplementary materials, which are designated by Tables S1 to S4 and Figures S1 to S4 and are available online at www.neoplasia.com.
[4] Contributed equally as first authors.
Received 14 November 2014; Revised 7 January 2015; Accepted 13 January 2015


1476-5586/15
http://dx.doi.org/10.1016/j.neo.2015.01.004

## Introduction

Lung cancer has a high incidence and mortality rate among human cancers globally [1]. There are many causes of clinical drug resistance resulting in recurrence and death; some of which may be attributed to ATP-binding cassette transporter family, such as ATP-binding cassette subfamily G member 2 (ABCG2) [2,3]. Increased ABCG2 expression promotes the exclusion of xenobiotics and their metabolites, thus protecting cancer cells from the toxic effects of the anti-cancer drugs [3,4].

ABCG2 is also used as a marker for cancer stem cells (CSCs) or cancer-initiating cells in various human cancers, including lung cancer [5,6]. CSCs represent a minor population of tumor cells with stem cell properties such as self-renewal and differentiation capacity. They are thought to be responsible for tumor initiation, propagation, resistance to chemotherapy, recurrence or regional spread, and distant metastasis [7]. Several molecular markers such as CD133 or CD44 are used to identify and purify CSCs. ABCG2, for example, has been shown to confer side population (SP) phenotype [8] to a subset of cancer cells that possess the features of CSCs [5]. Furthermore, the expression level of ABCG2 in the primary tumor can be used to predict prognostic outcome of patients with lung cancer [9,10]. Despite being used for CSC identification and purification, it remains largely unknown if and how these CSC markers confer CSCs with carcinogenic, invasive behaviors or other stemness properties.

Like many other CSC surface markers, ABCG2 proteins are thought to exist on the plasma membrane where they function to exclude xenobiotics from the cytoplasm. There are some reports describing possible localizations of ABCG2 on the membranes of mitochondria [11] or in the perinuclear region [12]. The presence of ABCG2 at these subcellular compartments is thought to facilitate substrate efflux from these organelles and therefore from inside the cell. In this report, we provide experimental evidence that ABCG2 proteins are also present inside the nucleus. Recently, several other localization studies have also demonstrated the possible presence of ABCG2 in the nucleus in head and neck squamous cell carcinoma cells, chorion trophoblasts, and glioblastoma multiforme cells [13–15]. However, it remains unclear whether these nuclear ABCG2 proteins are functional, and if so, what their functions are. We found that nuclear ABCG2 can serve as a transcription regulator of *CDH1*, the E-cadherin–encoding gene, and such transcriptional regulation, together and integrated with other regulators of epithelial-mesenchymal transition (EMT) or mesenchymal-epithelial transition (MET) pathways, can modulate multiple steps of cancer metastatic process.

## Materials and Methods

### *Cells and Cell Culture*

HEK-293T and A549 were obtained from the Bioresource Collection and Research Center of Taiwan (Hsinchu, Taiwan). HEK-293T cells were cultured in Dulbecco's modified Eagle's medium supplemented with 10% FBS (Invitrogen, Carlsbad, CA). A549 cells were cultured in Nutrient Mixture F-12 Ham supplemented with 10% FBS (Sigma-Aldrich, St Louis, MO). All cell lines were cultured at 37°C in a humidified atmosphere of 5% $CO_2$.

### *Immunofluorescence Staining*

Cells were seeded onto glass slides and fixed with 4% paraformaldehyde, permeabilized with saponin or Triton X-100, and subsequently incubated with the monoclonal ABCG2 primary antibodies 5D3 (1:50; Millipore, Darmstadt, Germany) or BXP21 (1:100; Santa Cruz Biotechnology, Dallas, TX) overnight at 4°C. The 5D3 antibody recognizes an external epitope of ABCG2, while the BXP-21 antibody was raised against amino acids 271 to 396 of ABCG2. Samples were then incubated with Alexa Fluor 488–conjugated goat anti-mouse IgG antibody (Invitrogen), and cell nuclei were stained with 4′,6-diamidino-2-phenylindole (DAPI; Sigma-Aldrich). Images were captured using a TCS-SP5 laser confocal microscope (Leica, Solms, Germany). Images were further digitally processed for contrast enhancement using Adobe Photoshop.

### *Extraction of Subcellular Fractions*

To examine the subcellular distribution of endogenous ABCG2, cells were fractionated using the ProteoExtract Subcellular Proteome Extraction kit (Calbiochem, Darmstadt, Germany) according to the manufacturer's instructions. Three fractions (fraction 1, cytosolic proteins; fraction 2, membrane and membrane organelles; and fraction 3, nuclear proteins) were collected and used for Western blot analysis.

### *Immunohistochemistry*

Lung cancer tissues were collected from Taipei City Hospital (Taipei, Taiwan) between 2011 and 2012; the experimental procedures followed the ethical regulations passed by the Institutional Review Board. We collected a total of 27 lung cancer tissues including 17 adenocarcinomas, 7 squamous cell carcinomas, 2 adenosquamous carcinomas, and one poorly-differentiated carcinoma. Immunohistochemistry was performed on 4-μm-thick paraffinized lung tissue specimens; sections were deparaffinized and rehydrated conventionally. For antigen retrieval, slides were immersed in Trilogy (Cell Marque Corp, Rocklin, CA) and boiled for 30 minutes in a pressure cooker. Endogenous peroxidase was blocked with 0.3% (vol/vol) $H_2O_2$ in methanol for 30 minutes. The slides were incubated with the primary anti-ABCG2 (BXP-21; Novus Biologicals, Littleton, CO) antibody overnight at 4°C. Thereafter, the slides were incubated for 1 hour with a polymer–HRP-labeled secondary antibody (DAKO EnVision$^+$ System). Diaminobenzidine tetrahydrochloride was used as a substrate. Next, the slides were counterstained with hematoxylin and scanned using a ScanScope CS (Aperio Technologies, Vista, CA).

### *Wound Healing Migration Assay, Transwell Migration, and Invasion Assay*

Confluent cells in culture dishes were scratched with a P1000 pipette tip and then washed several times to remove detached cells. Scratched cultures were photographed at 0 to 24 hours using an Olympus CKX31 inverted microscope (Olympus, Tokyo, Japan) equipped with a digital camera (Nikon, Tokyo, Japan). Cell migration was monitored by assessing closure of the wound and analyzed with ImageJ software. Migration was subsequently defined as the ratio of the open wound area after 0 to 24 hours to the initial wound area (% wound area = open wound area after different time points/initial wound area at 0 hour).

Transwell migration assays were performed using 12-well transwell migration chambers (8-μm pore size; Millipore). Invasion assays were performed using 24-well BioCoat Matrigel Invasion Chambers with 8-μm pores (BD Biosciences, San Jose, CA) according to the manufacturer's instructions. The detailed description is given in the Supplementary Methods.

### *Generation of the Reporter Construct and Luciferase Assay*

The pGL3–E-cadherin wild-type and mutant reporter plasmids were generated by modifying the pXP2–E-cadherin plasmid kindly provided by Dr. Muh-Hwa Yang [16]. The reporter constructs were

co-transfected into HEK-293T cells along with different expression or control vectors. A plasmid expressing the bacterial β-galactosidase gene (pCMV-βGal) was co-transfected in each experiment as an internal control. Cells were harvested after 48 hours of transfection; luciferase activity was measured in duplicate wells and normalized to β-galactosidase activity values to determine transfection efficiency. Experiments were repeated at least three times independently.

### *Chromatin Immunoprecipitation Assay*

To assess the binding of ABCG2 to the E-box region of the *CDH1* promoter, chromatin immunoprecipitation (ChIP) was performed using a ChIP assay kit (Millipore), according to the manufacturer's protocol. Polymerase chain reaction (PCR) and quantitative ChIP (qChIP) reaction generated a 201-bp product from the *CDH1* proximal promoter (−171 to +30) containing three E-box motifs (E1: −80 to −75; E2: −29 to −24, E3: +22 to +27) as described previously [16]. Primer sequences were given as follows: P1: 5′-TAGAGGGTCACCGCGTCTAT-3′ (forward) and P2: 5′-TCACAGGTGCTTTGCAGTTC-3′ (reverse).

### *Electrophoretic Mobility Shift Assay*

The electrophoretic mobility shift assay (EMSA) protocol was modified from previous reports [16,17]. Nuclear extracts (10 μg) were incubated with $1.7 \times 10^5$ cpm of [γ-$^{32}$P]-ATP end-labeled double-stranded oligonucleotides (E3: 5′-CTGCAAAGCACCTGTGAGCT-3′; E1: 5′-TGTGGCCGGCAGGTGAACCCT-3′; E2: 5′-GGGGCTCACCTGGCTGCA-3′) in 20 μl of binding buffer at 30°C for 20 minutes. For competition experiments, unlabeled oligonucleotides were added to the binding reaction mixture, which was placed on ice 20 minutes before addition of the radiolabeled probe. Addition of an antibody against the indicated protein resulted in the appearance of a supershift or impeded the protein-DNA binding.

### *Experimental Mouse Metastasis Model*

All mouse experimental procedures were approved by the Ethical Committee of Animal Experimentation of the National Yang-Ming University (Taipei, Taiwan). Six- to eight-week-old male nonobese diabetic-severe combined immunodeficiency (NOD-SCID) mice were purchased from the National Laboratory Animal Center (Taipei, Taiwan). Mice were housed under specific pathogen-free, temperature- controlled conditions. A549 stable cells (*ABCG2*-overexpressing cells, vector control cells, *shABCG2*-knockdown cells, and *shGFP*-control cells) were injected subcutaneously (s.c., $1 \times 10^7$) into the right side or intravenously (i.v., $1 \times 10^6$) into the tail vein of at least six NOD-SCID mice per condition. The mice were killed with $CO_2$ at 62 days (s.c. implanted) or after 6 weeks (i.v. injected). Subcutaneous tumors and lung tissue were surgically excised, weighed, and photographed. Tumor volume ($V$) was calculated by using the formula $V = 1/2 \times \text{length} \times (\text{width})^2$. The metastatic potential of A549 stable cell lines was evaluated from the number of lung nodules; number of nodules exceeding 200 was considered as 200.

### *Colony Formation Assay*

A549 stable cells (100 of each type) were suspended in culture medium and seeded in six-well culture plate, in triplicate. After culturing for 9 days, cells were fixed and stained with crystal violet, and viable colonies comprising more than 50 cells were counted.

### *Statistical Analysis*

All data are represented as means ± SD. Statistical differences between two data sets were compared by Student's $t$ test; non-parametric data were compared with the Mann-Whitney $U$ test, using GraphPad Prism software (v5.0, La Jolla, CA). Differences with $P$ values $<.05$ were considered statistically significant.

## Results

### *Nuclear Distributions of ABCG2 Proteins*

To further understand the subcellular distribution of ABCG2 proteins, we performed immunofluorescence staining on A549 human lung cancer cells using different fixation and permeabilization protocols (Figure 1*A*). Cells were fixed with 4% paraformaldehyde and treated with a relatively mild detergent, saponin; the subsequent 5D3 anti-ABCG2 antibody signals were predominant in the plasma membrane (white arrows) and cytoplasm (red arrows), the signals of which were clearly diminished due to Triton X-100 extraction. Signals of another ABCG2 monoclonal antibody, BXP21, were also observed virtually completely in the cytoplasm and nucleus (Figure 1*A*, *red arrows* and *white arrowheads*), with some signals in the plasma membranes (Figure 1*A*, *white arrows*) after saponin permeabilization. The nuclear pattern of BXP21 staining (Figure 1*A*, *white arrowheads*) was even more pronounced with a speckled distribution when cells were treated with Triton X-100. Moreover, the vertical sections in the *x-z* and *y-z* planes of confocal images further confirmed that ABCG2 was localized to the nucleus (Figure S1*A*). Irrespective of whether 5D3 or BXP21 antibody was used, the membrane patterns of ABCG2 staining were sensitive to Triton X-100 extraction. Intriguingly, the ABCG2 signal obtained with the 5D3 antibody, which recognizes an external epitope of the ABCG2 protein, was not observed in the nucleus, probably because nuclear ABCG2 undergoes a conformational change, resulting in a lack of recognition by the 5D3 antibody. We speculate that this is the reason why previous studies did not observe ABCG2 expression in the nucleus.

In addition to the localization study, we used subcellular fractionation and Western blot analysis experiments to quantify ABCG2 proteins in different subcellular compartments. As shown in Figure 1*B*, ABCG2 was not only found in the cytoplasm fraction (Cyto), which was marked by the presence of Hsp90α, glyceraldehyde-3-phosphate dehydrogenase (GAPDH), or β-tubulin, and the membrane fraction (Memb), which contained calnexin, but was also present in the nuclear fraction (Nu), which was enriched for nucleolar protein hNopp140. The longer exposure time of Figure 1*B* is shown in Figure S1*B*.

ABCG2 proteins were also found on the plasma membrane and inside the nucleus in another human lung cancer cell line CL1/TPT (Supplementary Methods). Immunofluorescence staining and cell fractionation studies showed that ABCG2 proteins were present not only in the cytoplasm and membrane fractions but also in the nuclear compartment (Figure S2). Note that the membrane form of ABCG2 was more abundant on the cell surface of CL1/TPT cells (Figure S2, *white arrows*) than A549 cells, which rendered CL1/TPT cells robustly resistant to the chemotherapeutic drug topotecan.

We also performed immunohistochemistry studies on clinical lung cancer tissues (Figure 1*C*). The ABCG2 expression patterns were divided into cytoplasmic/membranous pattern and nuclear pattern (Table S1). All membranous (exemplified by the top panel and inset in Figure 1*C*), cytoplasmic, and nuclear forms (exemplified by the bottom panel and inset in Figure 1*C*) of ABCG2 were found, at individually different proportions, in different regions of cancer tissues or among different patients. Among the 27 samples examined, 14 cases displayed discernible nuclear staining and the proportion of

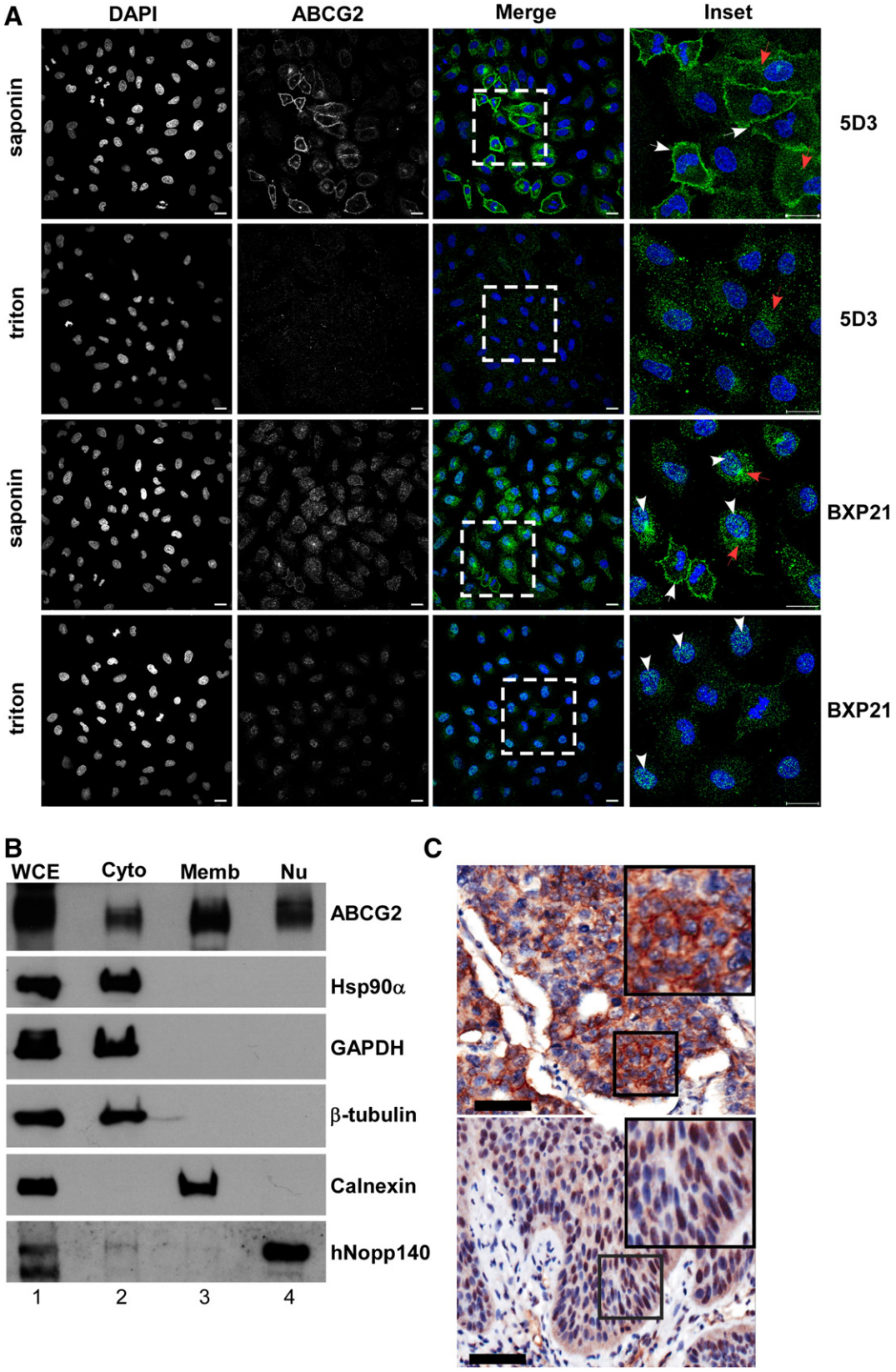


nuclear pattern was 51.9% (14/27). The nuclear or membranous ABCG2 localization did not significantly correlate with clinical diagnosis and prognosis (e.g., stage or survival). On further analysis, the percentage of nuclear staining cells in each case was found to be 1% to 30%. The high (≧10%) and low (<10%) percentage of nuclear staining cells in each case were categorized according to Table S1. The late stage (III and IV) patients showed higher proportion in high percentage of nuclear staining cells compared to early stage (I and II)

patients (3/5 *vs* 1/22). In addition, the late stage (III and IV) patients showed lower proportion in low percentage of nuclear staining cells compared to early stage (I and II) patients (2/5 *vs* 21/22). Significant difference was observed between percentage of nuclear staining and clinical stage, but no significant difference was observed between percentage of nuclear staining and survival; this is possibly because the number of our clinical tissues is insufficient (Table S2).

### *Additional Biologic Activities of ABCG2*

To elucidate the effect of ABCG2 expression, we established stable *ABCG2*-overexpressing and *ABCG2*-knockdown A549 clones whose ABCG2 expression was either overtly activated by overexpression or silenced by gene knockdown, respectively. SP cells constitute a cell population that excludes Hoechst dye from inside the cell (Figure 2*A*); these cells were selected by the dashed line and quantified as percentage at upper left corner of each flow analysis panel. Note that *ABCG2*-overexpressing cells contained more SP cells (34.8%) than vector control cells (20.8%) or parental cells (8.2%). In contrast, *ABCG2*-knockdown cells had fewer SP cells (1.5%) than *shGFP* control cells (10.9%). These results indicated that the exogenous ABCG2 proteins were functional and that the knockdown procedures were effective.

To understand how ABCG2 affects other biologic aspects of the cell, besides functioning as a membrane transporter, we investigated the general morphology and motility of A549 cells. A549 cells containing high levels of ABCG2 were more likely to adhere to each other and typically formed groups of cell clusters, than the parental cells or vector control cells, when observed under a microscope (Figure 2*B*, *arrows*). In contrast, *ABCG2*-knockdown A549 cells (*shABCG2*) were generally more dispersed throughout the entire growth substrate than the control cells; they seldom formed discernible cell clusters.

ABCG2 did not affect the rate of cell growth. Cell proliferation was comparable among the parental cells, *ABCG2*-overexpressing, and the vector control cells, and *ABCG2*-knockdown and *shGFP* control cells (Figure 2*C*).

We then examined if and how ABCG2 affected cell motility using both wound-healing (Figure 2, *D* and *E*) and transwell assays (Figure 2*F*). Since the rate of cell growth was not affected by ABCG2 (Figure 2*C*), we concluded that the difference observed in this set of wound-healing experiments was mainly due to the influence of ABCG2 on cell motility. The sequence of gap closure was exemplified by the microscopic images taken at representative time points, and the rate of wound-healing was quantified by the decrease of cell-free areas. Note that in parental or vector control cells, more than 70% of the gap had closed by 19 hours after wounding, whereas the gap remained largely unfilled in *ABCG2*-overexpressing cells even after 24 hours (Figure 2*D*). In contrast, knockdown of *ABCG2* significantly increased cell movement (Figure 2*E*). As the initial wound area of parental or vector control cells in Figure 2*E* was larger than that in Figure 2*D*, the gap had closed only 40% to 50% at 24 hours after wounding. However, the rate of gap closure in *shABCG2* cells was markedly faster than that in parental or *shGFP* control cells.

Furthermore, in a series of transwell migration assays, the amount of cells migrating to the opposite side of the transwell membrane was examined and quantified under microscopy. *ABCG2*-overexpressing cells exhibited a 60% decrease in transwell migration, compared to the control cells, whereas the *ABCG2*-knockdown cells demonstrated a 20% increase relative to the control (Figure 2*F*).

### *Expression Level of ABCG2 Is Correlated with Genes Related to Cell Adhesion and Motility*

ABCG2-modulated genes were identified from co-expressed genes in an expression microarray. ABCG2 expression levels were controlled by *ABCG2* overexpression (*ABCG2*), knockdown (*shABCG2*), or control vectors (Vec-ctrl or *shGFP*) in three independent experiments. The average *ABCG2* expression levels of each treatment are shown in Figure S3. *ABCG2*-overexpressing cells had the highest expression level, while *shABCG2*-knockdown cells showed the lowest expression level, and both controls (Vec-ctrl and *shGFP*) had similar and intermediate expression levels. We identified highly co-expressed genes according to Pearson correlation coefficient between test probe and *ABCG2* (209735_at).

The top 100 positively/negatively correlated probes (Table S3) were selected and represented 135 genes. We then performed gene ontology (GO) analysis on the gene list by using the online software DAVID [18]. A total of 41 enriched GO terms was highlighted at the default threshold, including the terms cell adhesion, growth regulation, cell development, cellular response to stress, intracellular transporter, and so on (Table S4). In the term list, cell adhesion (GO:0007155, $P < .05$) was the most frequently annotated function (13/135 genes), consistent with previous cell morphologic observations that reported that compact cell clusters are found in *ABCG2*-overexpressing cells (Figure 2*B*). Among the 13 genes related to cell adhesion (data not shown), E-cadherin (*CDH1*), a key cell-cell adhesion gene, was found to correlate strongly with *ABCG2* ($r > 0.9$, $P < 5 \times 10^{-5}$, Figure 3*A*, *left*). E-cadherin level is a hallmark in EMT or MET (reverse EMT) regulation [19]. We also observed that the mesenchymal marker, N-cadherin (*CDH2*), had a negative correlation with ABCG2 ($r < -0.6$, $P < .05$, Figure 3*A*, *right*). This implies that *ABCG2*-overexpressing cells retained the phenotype of epithelial cells by increasing *CDH1* and decreasing *CDH2*. Co-expression of *CDH1* and *ABCG2* at mRNA and protein levels were also confirmed using quantitative reverse transcription (QRT)–PCR (Figure 3, *B* and *C*, and S2*C*) and Western blot analysis (Figure 3*D*), respectively. These results suggest that ABCG2 modulates E-cadherin expression in A549 and CL1/TPT cells.

Furthermore, we also investigated other epithelial markers, claudin-1 and ZO-1, and the mesenchymal markers, N-cadherin and vimentin. When *ABCG2* was knocked down, both claudin-1 and

**Figure 1.** The localization and expression of endogenous ABCG2 in A549 cells and lung cancer tissues. (**A**) A549 cells were fixed with paraformaldehyde and permeabilized with saponin or Triton X-100, and then stained with 5D3 or BXP21 anti-ABCG2 antibody (green). Nuclei were stained with DAPI (blue). The inset is the zoom-in of the area highlighted with white dash line square box. White arrows indicate the plasma membrane, red arrows indicate the cytoplasm, and white arrowheads indicate nuclear signals. Scale bar, 20 $\mu$m. (**B**) Subcellular distribution of ABCG2 in A549 cells. Whole cell (WCE, lane 1), cytoplasmic (Cyto, lane 2), membranous (Memb, lane 3), and nuclear (Nu, lane 4) extracts were prepared from A549 cells and used in Western blot analysis for the detection of ABCG2, using BXP21 anti-ABCG2 antibody. Hsp90α, GAPDH, and β-tubulin were used as cytoplasmic fraction makers; calnexin was used as a membrane marker, and hNopp140 was as a nuclear marker. (**C**) Immunocytochemistry of lung cancer tissues showing significant ABCG2 expression in the cytoplasm/membrane, without nuclear expression (top panel, inset) and nuclear ABCG2 staining (bottom panel, inset) in different squamous cell carcinoma specimens. Scale bar, 50 $\mu$m.

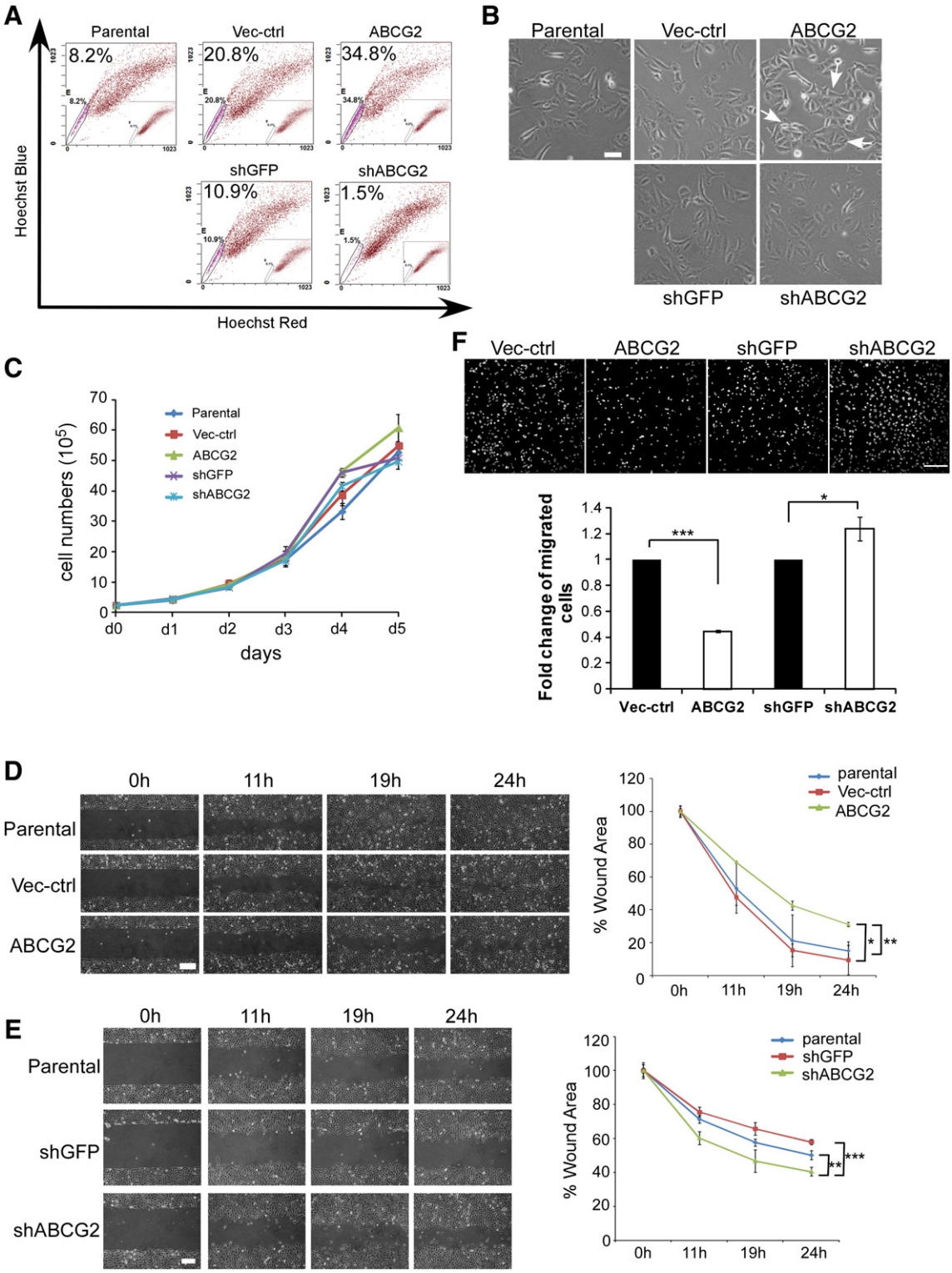


ZO-1 levels were decreased, and N-cadherin levels were increased; however, no perceptible changes in these markers were observed in *ABCG2*-overexpressing cells (Figure 3*D*). The vimentin levels remained unchanged in ABCG2 knockdown and overexpressing cells. These findings indicated that ABCG2 may be partially involved in EMT or MET regulation, particularly in E-cadherin modulation.

### *ABCG2 Is Involved in Transcriptional Regulation of CDH1*

ABCG2 overexpression enhances E-cadherin expression as well as increased nuclear ABCG2 expression (Figure S4*A*, *left*). The ratio of nuclear/cytoplasmic (N/C) ABCG2 protein levels in *ABCG2*-overexpressing cells was also increased (Figure S4*A*, *right*), whereas the nuclear ABCG2 or ratio of N/C ABCG2 protein levels was

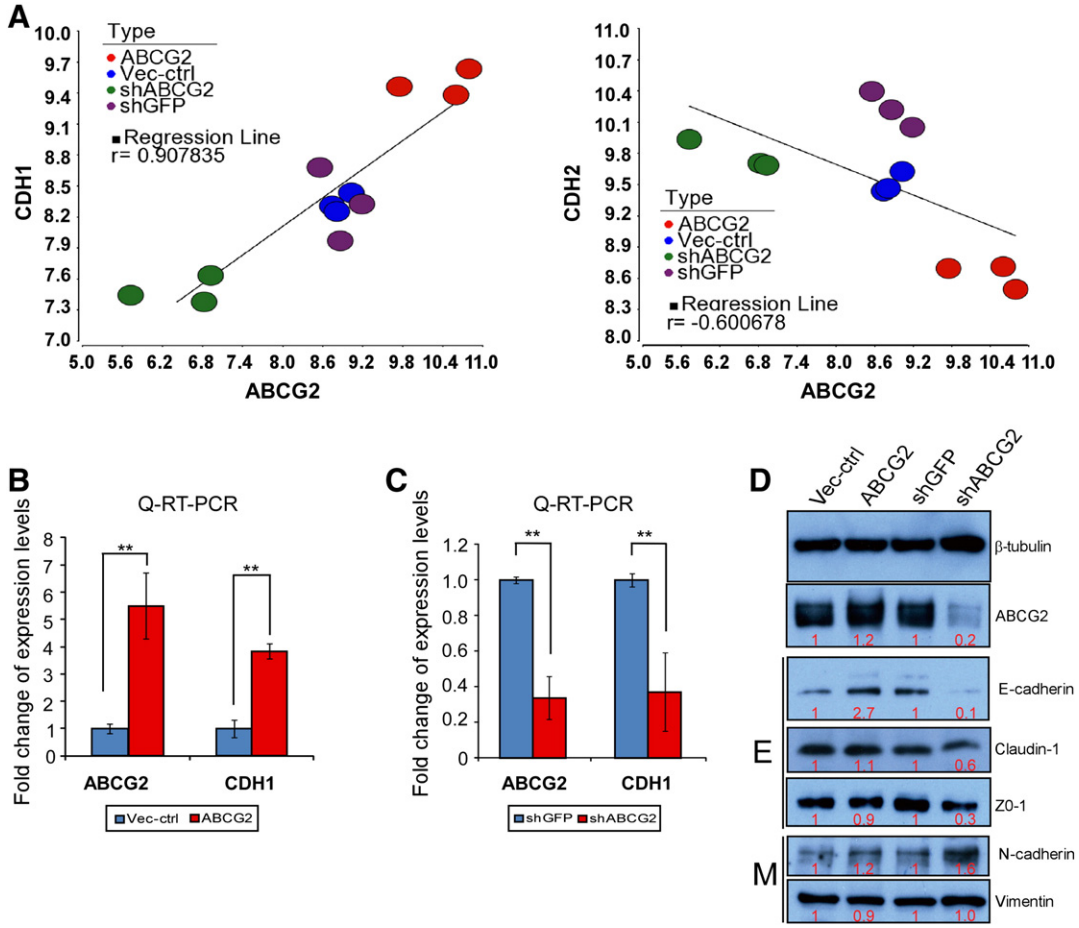


**Figure 3.** ABCG2 affects expression of EMT or MET markers in A549 cells. (**A**) The ABCG2 expression levels of four A549 stable cell lines (Vec-ctrl, *ABCG2*, *shGFP*, or *shABCG2*) in microarray experiments. (Left) Expression levels of *ABCG2* (*X*-axis) and *CDH1* (*Y*-axis) show a strong positive correlation in microarray experiments. (Right) Expression levels of *ABCG2* (*X*-axis) and *CDH2* (*Y*-axis) were negatively correlated. (**B** and **C**) mRNA levels of *ABCG2* and *CDH*1 were measured by QRT-PCR. *ABCG2* and *CDH1* levels had increased five- and four-fold in *ABCG2*-overexpressing cells, respectively. Both genes were decreased three-fold in *ABCG2*-knockdown cells. Average fold changes ($n = 3$) are shown in the bar chart; $^{**}P < .01$. (**D**) Western blot analysis of ABCG2 and EMT markers in A549 stable cells. Epithelial markers (E): E-cadherin, claudin-1, and zona occludens (ZO-1); mesenchymal markers (M): N-cadherin and vimentin. β-Tubulin was used as a loading control. The number at the bottom of each column is the fold change of quantitative protein level normalized to β-tubulin compared with the control.

decreased in the *shABCG2* cells (Figure S4*B*). We hypothesized that nuclear ABCG2 could regulate *CDH1* transcription by binding to the *CDH1* promoter and thereby regulate E-cadherin expression and inhibit cell migration. Three E-box motif sequences, CANNTG (E1, E2, and E3), were identified in the proximal (−147 to +60 base pairs) promoter region of *CDH1* [16]. We therefore generated a reporter construct containing the E-box wild-type (CAGGTG) or mutant (ACTTCA) motif of the *CDH1* promoter and tested its activation by ABCG2 (Figure 4*A*). An increase in wild-type *CDH1* promoter activity was observed in *ABCG2*-overexpressing cells, while Snail, a negative regulator of *CDH1*, clearly suppressed the promoter activity. Mutation of all three E-boxes abolished the activation by ABCG2 and

**Figure 2.** ABCG2 affects SP percentage, cell morphology, and motility in A549 cells. (**A**) Hoechst staining and flow cytometric identification of SP cells in A549 parental, vector control (Vec-ctrl), *ABCG2*-overexpressing (*ABCG2*), shRNA knockdown control (*shGFP*), and *ABCG2*-knockdown (*shABCG2*) cells. The SP cell gating area, treatment of cells with the ABCG2 inhibitor, fumitremorgin C, and the disappearance of SP cells after treatment with fumitremorgin C are indicated in the lower right quadrant of each panel. (**B**) Comparison of cell morphology in parental or stable A549 cells (Vec-ctrl, *ABCG2*, *shGFP*, and *shABCG2*). Arrows indicate cell clusters. Scale bar, 50 μm. (**C**) Comparison of cell growth in parental or stable A549 cells (Vec-ctrl, *ABCG2*, *shGFP*, and *shABCG2*). Equal number of cells was cultured in tissue culture plates for 5 days. After the indicated times, viable cells were counted after trypan blue staining. Error bars represent the SD from three independent replicates. (**D** and **E**) Wound-healing migration assay in parental and stable A549 cells (Vec-ctrl, *ABCG2*, *shGFP*, and *shABCG2*). (Left) Photos of wound-healing assay at different time points. (Right) Relative wound area at different time points. Values are expressed as percentage of the initial wound area. Scale bar, 100 μm. (**F**) Migration of A549–Vec-ctrl, *ABCG2*, *shGFP*, and *shABCG2* cells through uncoated transwell membranes. After 12 hours, the migrated cells were fixed, stained, and photographed. Representative photographs of transwell membranes showing stained migrated cells in motility experiments (top panel). The relative migratory ability of the indicated cells is displayed in the bottom panel. Values shown are means ± SD of three independent experiments. Scale bar, 100 μm. $^{*}P < .05$, $^{**}P < .01$, and $^{***}P < .001$.

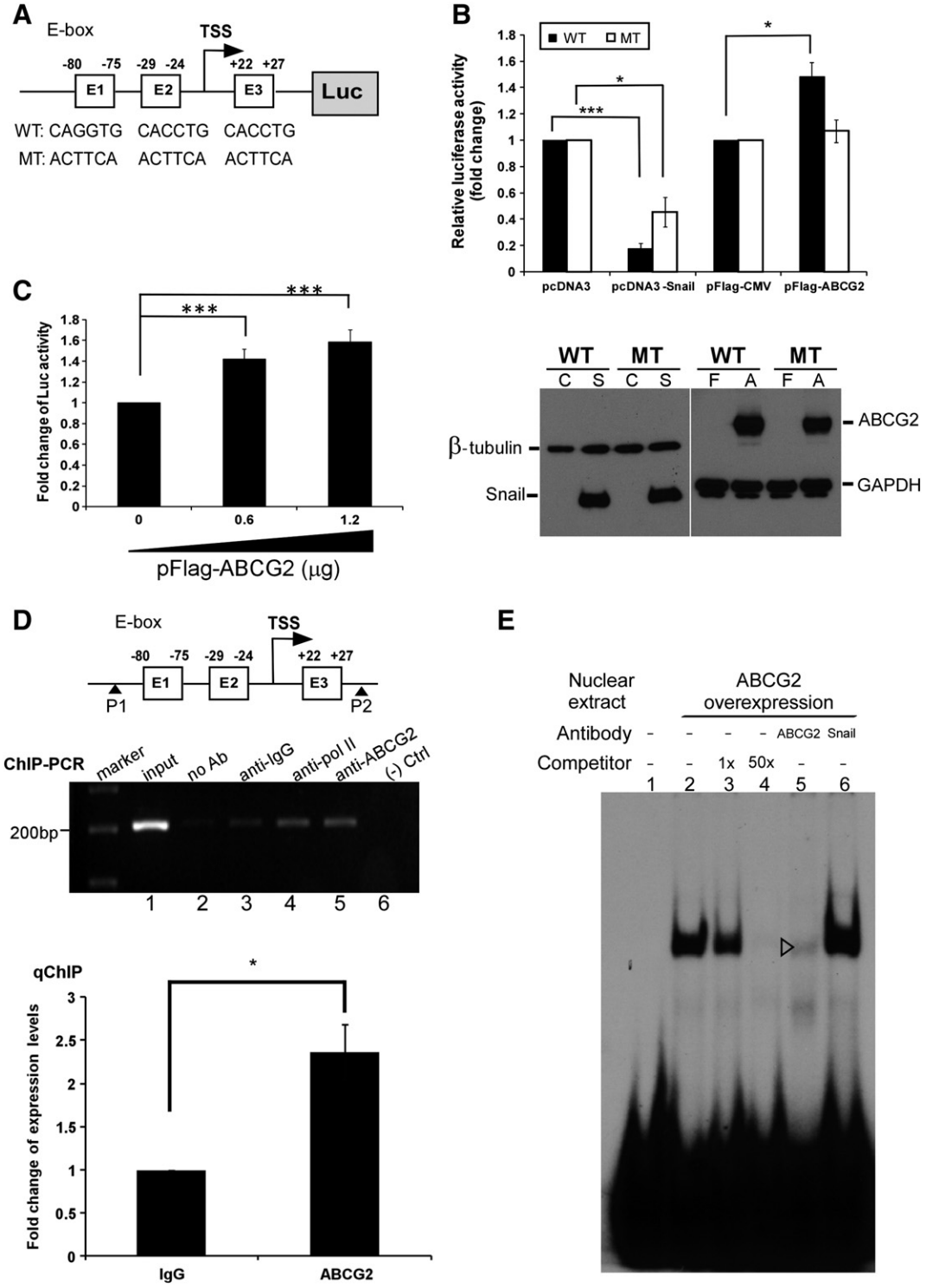


reversed the repression from 82% to 55% by Snail (Figure 4*B*, *top*); Western blot analysis confirmed the expression of ABCG2 and Snail in wild-type and mutant reporter experiments (Figure 4*B*, *bottom*). Furthermore, ABCG2 upregulated the promoter activity of *CDH1* in a dose-dependent manner (Figure 4*C*).

We further investigated the interaction between *CDH1* promoter and ABCG2 by ChIP analyses in *ABCG2*-overexpressing cells. The presence of the *CDH1* promoter in the precipitated complex was determined by PCR amplification, using primers specific for a 201-bp segment of the proximal portion of the *CDH1* promoter (Figure 4*D*). This PCR amplicon, containing the E-box motif, was increased in the sample precipitated with the BXP21 anti-ABCG2 antibody (Figure 4*D*, *lane 5*) compared with the no-antibody control (Figure 4*D*, *lane 2*) and mouse IgG control (Figure 4*D*, *lane 3*). qChIP demonstrated a two-fold increase in the binding of ABCG2 to the *CDH1* promoter, as compared with the mouse IgG control (Figure 4*D*, *bottom*).

Furthermore, EMSA was performed to confirm that ABCG2 can bind to the *CDH1* E-box motif. ABCG2-binding activity increased after incubation of nuclear extracts from *ABCG2*-overexpressing cells with the labeled E3 box-containing oligonucleotide (Figure 4*E*, *lane 2*), and ABCG2-binding activity was specifically competed by 1- or 50-fold unlabeled E3-box oligonucleotides (Figure 4*E*, *lanes 3* and *4*). Moreover, use of the BXP21 anti-ABCG2 antibody in the binding reaction markedly reduced the level of the binding complex (Figure 4*E*, *lane 5*), while no detectable change was observed with anti-Snail antibody (Figure 4*E*, *lane 6*), indicating that the ABCG2 antibody recognizes ABCG2 protein epitope that also contains ABCG2 protein-DNA binding region. This antibody impedes ABCG2 protein binding to DNA, so the supershift band was not observed. Similar results were observed when the E1- or E2-box oligonucleotide was used for EMSA (data not shown). Thus, these results demonstrated that ABCG2 activated *CDH1* transcription by binding to the E-boxes of the promoter.

### *ABCG2 Attenuates Invasiveness but Promotes Colonization of Circulating Cancer Cells*

We next investigated the impact of ABCG2 on tumor growth and the metastatic ability of four A549 stable cell lines using a mouse xenotransplantation assay. *ABCG2*-overexpressing, *ABCG2*-knockdown, and their control cells were injected s.c. or i.v. into NOD-SCID mice. The subcutaneous tumor volumes in the four groups were not significantly different after 62 days (Figure 5*A*, *left*). To determine the impact of ABCG2 on distant metastases after the formation of the primary subcutaneous tumors, we performed a detailed survey in the four groups of mice after sacrifice. One lung nodule was identified in one of eight mice in the *ABCG2*-overexpressing group; six lung nodules were found in one of six mice in the vector control group (Figure 5*A*, *middle*, *arrowhead*); three mice in the *shABCG2* group showed metastasis [two mice had five and eight lung nodules, respectively, and one mouse had one colon nodule (Figure 5*A*, *left*, #, and *right*, *arrowhead*)]; and no metastases were observed in the *shGFP* group (Figure 5*A*). Although there was a higher frequency (3/9; 30%) of metastasis in mice injected with *shABCG2* cells compared to those injected with the *shGFP* control (0/8; 0%) or the other two groups (ABCG2: 1/8; 12.5%, Vec-ctrl: 1/6; 16.7%), there was no correlation between tumor volume and metastasis frequency. These data imply that knockdown of *ABCG2* promoted invasion of lung or colon tissue. Similarly, *ABCG2*-knockdown cells had a higher invasion capacity in the *in vitro* invasion assay (Figure 5*B*). The *shABCG2* cells increased their invasion ability two-fold, while *ABCG2*-overexpressing cells decreased their invasion ability compared to their control cells. All of these findings indicated that knockdown of *ABCG2* increased invasive ability and conferred distant metastases.

Simultaneously, we also determined the capacity for colonization in circulating cancer cells by i.v. injection, bypassing the initial steps of metastasis. We observed and quantified the number of lung nodules at 6 weeks after i.v. injection using four A549 stable cell lines (Figure 6, *A* and *B*). Nodules produced by *ABCG2*-overexpressing cells became confluent on the surface of the lung tissue. The median number of lung nodules in the recipients of *ABCG2*-overexpressing cells was 183 (range: 105-200, $N = 9$), vector control cells was 33 (range: 7-68, $N = 9$), *ABCG2*-knockdown cells was 82 (range: 21-150, $N = 9$), and *shGFP* control cells was 23 (range: 6-38, $N = 9$). *ABCG2*-overexpressing cells had a greater ability to colonize the lungs than Vec-ctrl ($P < .0001$) or *shABCG2* ($P < .0001$) cells *in vivo* (Figure 6*B*). Moreover, *ABCG2*-overexpressing cells had a greater ability to form colonies *in vitro* than did the other three groups (Figure 6*C*). Although we observed that the colonization ability of *ABCG2*-knockdown cells was far lower than that of *ABCG2*-overexpressing cells, it remained higher than that of *shGFP* control cells *in vitro* and *in vivo*. Because the *shABCG2* cells have a lower E-cadherin level (Figure 3, *C* and *D*) and higher motility (Figure 2*F*) than *shGFP* control cells, *shABCG2* cells may favor localized migration and cause more lung nodules or greater colony number than *shGFP* control cells. These results demonstrated that *ABCG2* overexpression decreases invasiveness but promotes lung colonization. The study implies that the epithelial-type cells in circulation favor to colonize in the late stage of the metastatic process.

## Discussion

We report here that, in addition to the known transport functions on the plasma membrane, ABCG2 is also present inside the nucleus where it plays a novel role in modulating *CDH1* transcription, similar to the previous report that the epidermal growth factor receptor (EGFR) can translocate to nucleus and serve as a transcription factor to regulate ABCG2 expression [20]. In Figure 7, most ABCG2 proteins synthesized are translocated to the plasma membrane ①,

**Figure 4.** ABCG2 enhances *CDH1* transcription by binding to the E-boxes of the *CDH1* promoter. (**A**) Schematic representation of the promoter region of the wild-type (WT) or E-box–mutated (MT) *CDH1*. TSS, transcription start site. E1, E2, and E3 indicate the location of E-boxes. (**B**) Promoter activity assay in HEK-293T cells transfected with various constructs (top). The promoter luciferase activities of these cells were normalized to that in control cells transfected with the empty vectors (pcDNA3 or pFlag-CMV). Western blot analysis confirmed the expression of ABCG2 and Snail in cells transfected with various constructs. C: pcDNA3 vector, S: pcDNA3-Snail, F: pFlag-CMV vector, and A: pFlag-ABCG2. (**C**) ABCG2 upregulated the promoter activity of *CDH1* in a dose-dependent manner. Cells were transfected with increasing amounts of pFlag-ABCG2 expression vector, as indicated. Values shown are means ± SD from at least three independent experiments. $*P < .05$, $***P < .001$. (**D**) Top: Schematic representation of the promoter region of *CDH1* and P1 and P2 paired primers (arrowhead). P1 and P2 specifically amplified a 201-bp fragment containing the E-box region of *CDH1* in ChIP-PCR or qChIP. Middle panel: ChIP-PCR gel image. Fragmented chromatin was incubated either without antibodies (no Ab, lane 2), with anti-IgG isotype antibody (lane 3), anti-polymerase II antibody (pol II, lane 4), or anti-ABCG2 antibody (lane 5) and was then subjected to PCR using P1 and P2 primers to amplify a 201-bp fragment in A549 *ABCG2*-overexpressing cells. Pol II was used as control for the ChIP experiment. Lane 1 represents the total DNA input (positive control), whereas (–) Ctrl (lane 6) represents the negative control subjected to PCR. Bottom: Fold change in chromatin enrichment indicated by QRT-PCR data, as compared with anti-ABCG2 antibody and isotype IgG in A549 *ABCG2*-overexpressing cells. Values shown are the means ± SD from three independent experiments. $*P < .05$. (**E**) ABCG2 binds to the E-box (E3) region of the *CDH1* promoter using EMSAs. Lane 1: no protein extract. Competition assays were performed to test the specificity of binding of nuclear proteins with the probe. Incubation of the labeled E3-box oligonucleotides with nuclear extracts alone (lane 2), in the presence of 1-fold (lane 3) or 50-fold (lane 4) of unlabeled E3-box oligonucleotides, is shown. Protein-DNA interactions are denoted by the appearance of one specific band (lanes 2, 3, and 6). Addition of the anti-ABCG2 antibody results in impediment to protein-DNA interaction (lane 5, open arrowhead); Snail antibody was used as a control (lane 6).

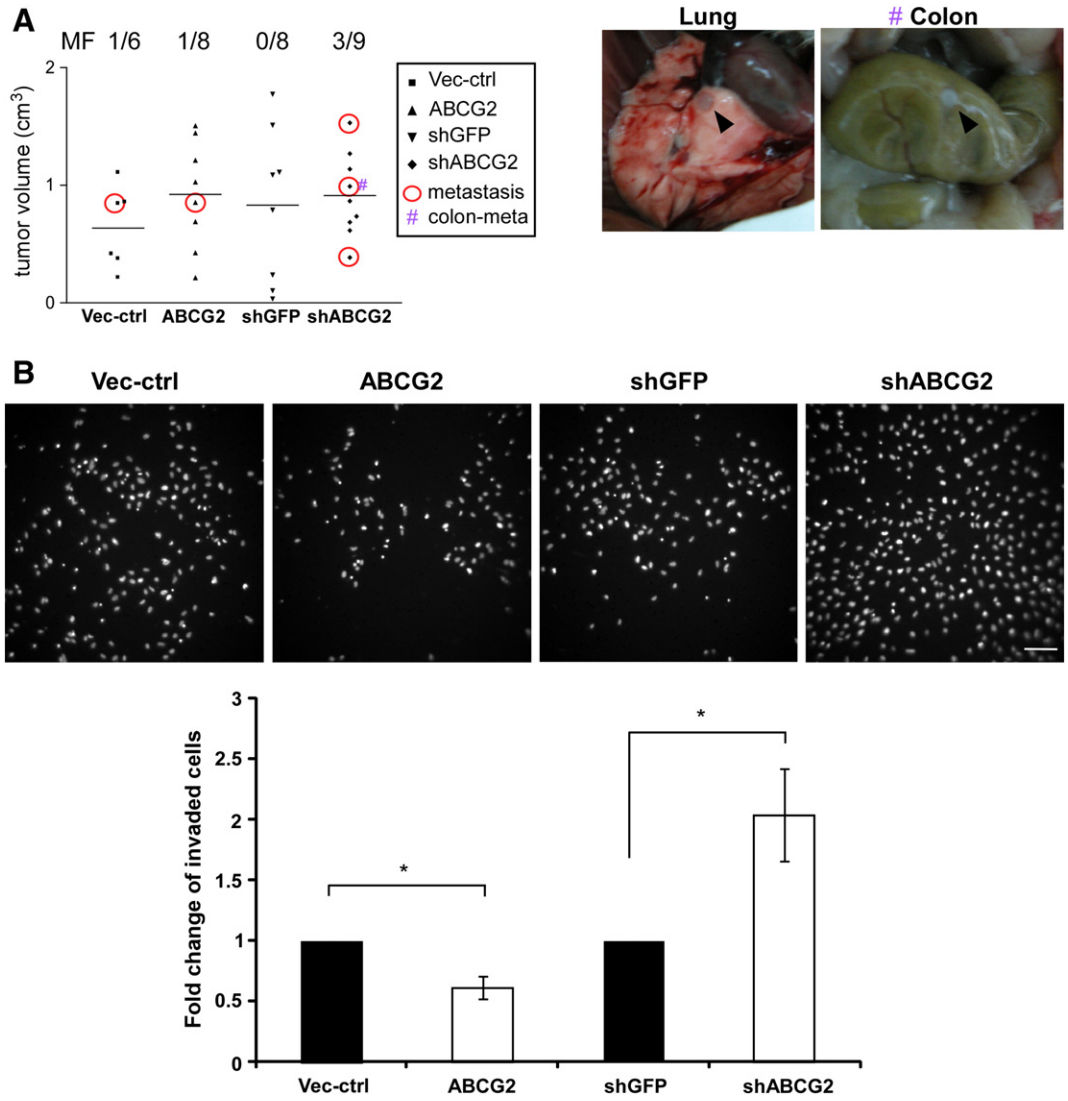


**Figure 5.** ABCG2 attenuates invasiveness *in vivo* and *in vitro*. (**A**) The volume of subcutaneous tumors following injection of $1 \times 10^7$ *ABCG2*-overexpressing, Vec-ctrl, *shABCG2*, or *shGFP* stable cells into NOD-SCID mice. The horizontal line indicates the mean of tumor volume. Red circles indicate mice showing metastasis; # indicates a mouse possessing a colon metastatic nodule. The fraction of mice developing metastases (MF) in individual groups is represented above. Middle and right representative image of metastatic nodules (arrowhead) is in lung or colon tissue in different mice, respectively. (**B**) Invasive ability of A549–Vec-ctrl, *ABCG2*, *shGFP*, and *shABCG2* cells was examined using Matrigel-coated transwells. After 65 hours, the migrated cells were fixed, stained, and photographed. Representative images of a transwell insert showing stained invasive cells (top panel). The relative invasive ability of the indicated cells is displayed in the bottom panel. Values shown are means ± SD from three independent experiments. Scale bar, 100 $\mu$m. *$P < .05$.

where they function to exclude xenobiotics from the cytoplasm and, by doing so, confer the cell with SP phenotype. Our localization and cellular fractionation studies (Figure 1), and functional data (Figure 4), showed an unexpected distribution of ABCG2 inside the nucleus ②. The ABCG2-shuttling mechanism between the plasma membrane and cytoplasm has been investigated. Xie et al. demonstrated that Pim-1 phosphorylates ABCG2 at Thr362 and thereby enables its translocation to the cell surface [21]. Moreover, the phosphatidylinositol-3-kinase (PI3K)-AKT signaling pathway could regulate ABCG2 translocation from the plasma membrane to intracellular compartments and could affect efflux activity and SP [22–24]. In addition, Huang et al. demonstrated that activated Akt could phosphorylate EGFR and facilitate increased nuclear EGFR that act as transcription factors to mediate ABCG2 expression in gefitinib resistance cells [20]. Whether AKT and/or Pim-1 activity modulate ABCG2 shuttling between the cytoplasm and nucleus requires further investigation. Although ABCG2 lacks the conventional nuclear localization signal (NLS) for import into the nucleus, ABCG2 contains four lysine residues at positions 357 to 360, which may act as a putative NLS through interaction with specific receptors at nuclear pores [15]. It is also possible that ABCG2 is co-transported into the nucleus by binding to other nuclear or accessory molecules. Moreover, the EMSA results (Figure 4*E*) indicated that the specific binding complex was obstructed by the BXP21 anti-ABCG2 antibody that recognizes the intracellular region (271-396 amino acid [aa]), which contains the four lysine residues of the putative NLS. We speculate that this intracellular region (271-396 amino acid [aa]) of ABCG2 may be involved in DNA binding so the supershift band

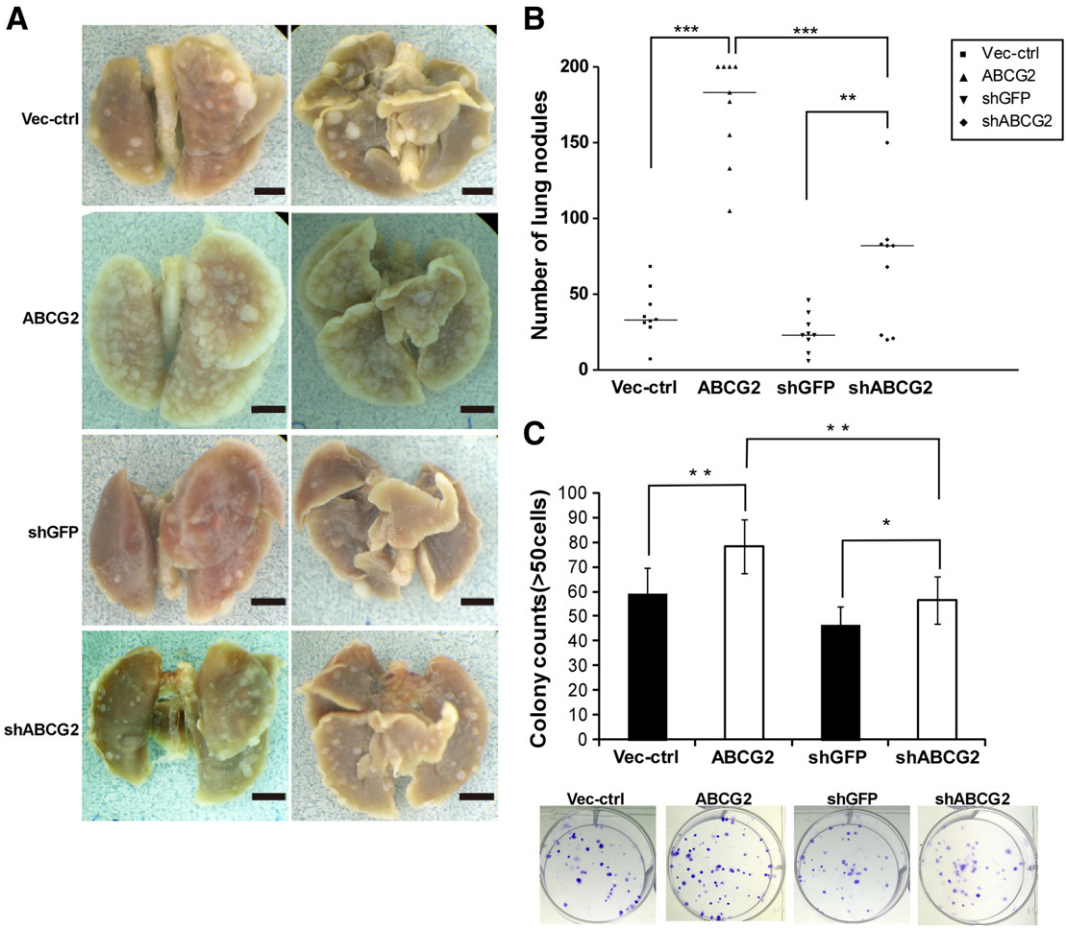


**Figure 6.** ABCG2 promotes lung colonization *in vivo* and *in vitro*. (**A** and **B**) Images of lung tissues and quantification of lung nodules per mouse at 6 weeks after tail vein injection. The number of lung nodules in mice injected i.v. with $1 \times 10^6$ of stable A549 cells (Vec-ctrl, *ABCG2*, *shGFP*, or *shABCG2*). The horizontal line indicates the median of lung nodules. Scale bar, 2.5 mm. Each dot represents a single mouse. Student's *t* test was used to compare the average number of events per group. $^{**}P < .01$, $^{***}P < .001$. (**C**) Colony formation assay of A549 stable cells. Colonies larger than 50 cells were counted. Bottom: Representative images of colonies. Data represents means ± SD from three independent experiments. $^{*}P < .05$, $^{**}P < .01$ by Student's *t* test.

was not observed. We are generating several truncated fragments of ABCG2 and will be using them to verify their cellular distribution. In future, we will confirm the region of the ABCG2 sequence that is responsible for nuclear translocation or DNA binding.

In this study, we have verified that ABCG2 is present in the nucleus of A549 cells, CL1/TPT lung cancer cells, and clinical tissues (Figures 1 and S2). Additionally, it is interesting that ABCB1, another ATP-binding cassette transporter, was also previously demonstrated to locate to the nucleus [25]. Moreover, some studies have shown that ABCG2 is located in the nucleus in different cell types, by immunohistochemistry, immunofluorescence, or fractionation experiments [13–15]. These studies all indicate that nuclear ABCG2 plays an important role in efflux of substrates from the nuclear compartment. However, these reports did not discuss the molecular mechanism by which nuclear ABCG2 may affect gene regulation. In our studies, we not only demonstrated that ABCG2 localizes to the nucleus but also evaluated the molecular mechanisms involving nuclear ABCG2 in A549 cells. Our immunofluorescence analysis employed different degrees of permeabilization and different antibodies (5D3 and BXP21) to further confirm ABCG2 nuclear localization (Figure 1). Different signal patterns were observed, due to recognition of different regions of ABCG2. It is a possible that conformational changes, rather than alternative splicing, are involved in nuclear ABCG2, because Western blot analysis of cellular fractions showed that the molecular weight of nuclear ABCG2 is equal to that of membrane ABCG2 (Figure 1*B*).

After entering the nucleus, ABCG2 can bind to the E-box promoter region of *CDH1* and upregulate E-cadherin transcription ③. Several well-known transcription factors bind to the *CDH1* promoter and participate in the control of E-cadherin expression, such as AP-2 and WT-1 bind to GC-rich region to activate transcription [26,27], and Snail, Slug, SIP1, and Twist1 bind to the E-box element to repress gene expression [28–32]. E-box elements were thought to play a critical negative regulatory role in *CDH1* transcription. A breakthrough finding in our study was that nuclear ABCG2 positively regulated *CDH1* expression through E-box elements of the promoter. We do not yet know if and how ABCG2 interacts and/or coordinates with these transcription factors to regulate E-cadherin expression in the cancer cells. Nuclear ABCG2 may act as a competitor against these repressors by binding to E-box element of *CDH1* promoter and decreasing E-cadherin repression. The dynamic interplay between these well-known transcription factors and ABCG2 on the *CDH1* promoter remains elusive and needs to be unraveled.

E-cadherin is a well-established tumor invasion suppressor [33]. Complex and dynamic transcription regulation is the major mechanism

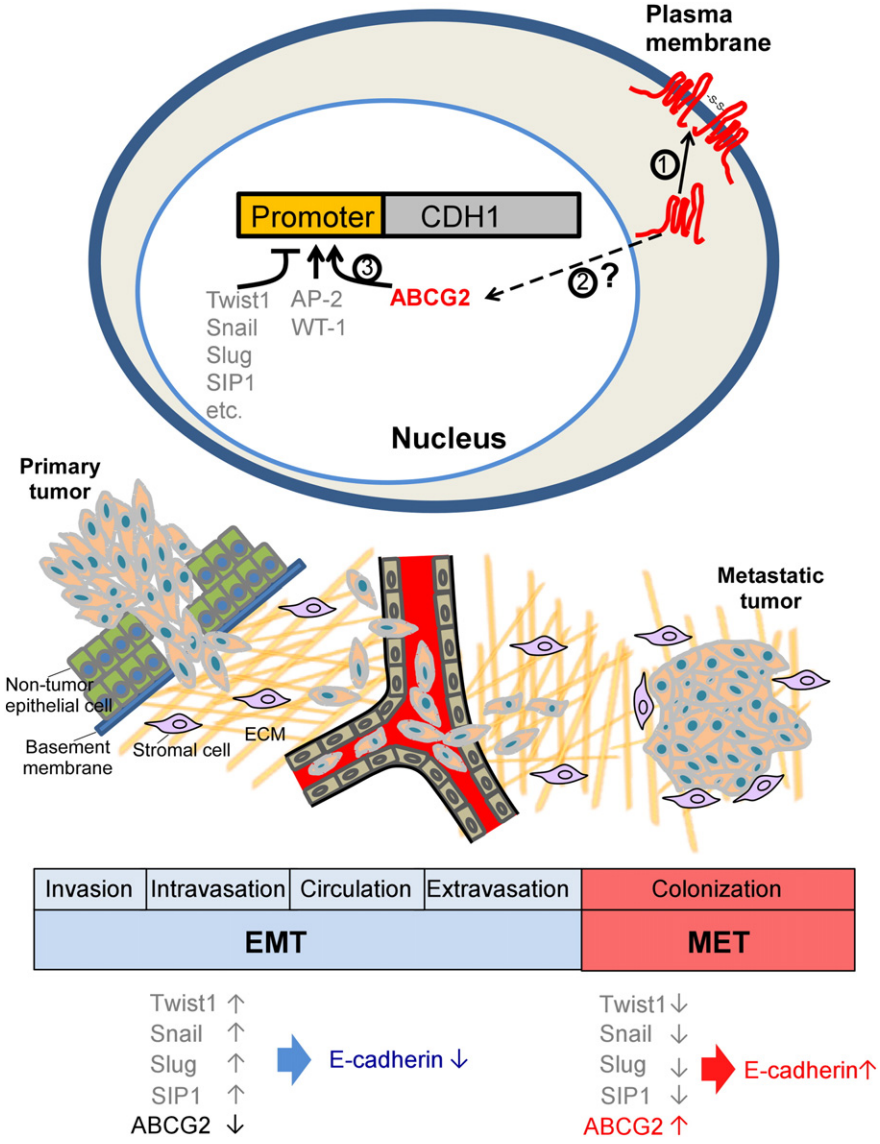


**Figure 7.** Proposed metastasis model summarizing the role played by nuclear ABCG2 in upregulating *CDH1* transcription and trending MET progression in this study. ABCG2 localizes to the nucleus and activates *CDH1* transcription by binding to promoter region (Top) ②③. The Twist1, Snail, Slug, SIP1, and so on participates in EMT and MET progression by regulating the *CDH1* transcription. ABCG2 overexpression causes increased E-cadherin and promotes tumor cell colonization, and subsequently form macrometastases (bottom). See Discussion section for detailed description. ECM: extracellular matrix.

of controlling E-cadherin expression that govern the EMT or MET progression [19]. E-cadherin plays a pivotal role in many steps during cancer metastasis, especially those involved in primary tumor invasion (i.e., penetration of the carcinoma cells through the basement membrane), entering and leaving the blood stream (intravasation-circulation-extravasation), and then the formation of a metastatic tumor (colonization) at a distant site (Figure 7, *bottom*). Extensive studies have made it clear that decreased expression of E-cadherin, due to suppression of *CDH1* by transcription repressors, is advantageous for EMT of the cancer cells to undergo invasion, intravasation, circulation, and extravasation progression [28–32,34]. However, for migrating cancer cells to form a metastatic tumor at a distant site, cells need to settle, recolonize, and grow when high expression of E-cadherin in the cancer cells can promote MET progression [35,36]. Recent studies have shown that silencing of one repressor (such as SIP1, ZEB1, or Twist1) could upregulate E-cadherin expression that may play a critical role in tumor colonization [37–39]. How ABCG2 is involved in metastatic progression is currently unclear. In our study, we found that not only does nuclear ABCG2 positively regulate E-cadherin expression and enhance metastatic colonization, but overexpressed ABCG2 can also cause lowering of Snail and SIP1 expression in A549 cells (data not shown). In addition, *ABCG2* may negatively regulate the *CDH2* expression that could contribute to the metastatic process (Figure 3, *A*, *right*, and *D*). Thus, we observed most numerous lung nodules in xenografted mice, after i.v. injection of *ABCG2*-overexpressing cells.

Several lines of evidence have indicated that ABCG2 plays a crucial role in protecting stem cells from death, cytotoxic substrates, and maintained homeostasis under stress condition or undifferentiated state [40–42]. In our study, *ABCG2*-overexpressing cells contained more SP cells with an epithelial phenotype (Figure 2) and were demonstrated to have a higher lung metastatic colonization in the mouse model (Figure 6), suggesting that some SP cells, a CSC-enriched population,

have higher ABCG2 expression and tend to activate MET progression. Recent studies supporting our findings have shown that highly metastatic CSCs express a strong epithelial gene profile and that epithelial-type cells promote tumor colonization and proliferation [43,44]. MET was demonstrated to be essential for efficient metastatic colonization [45,46] and generation of induced pluripotent stem cells [47,48]. Additionally, Chang et al. demonstrated that connective tissue growth factor induces the MET process and stem-like properties, promoting local progression and reducing invasiveness in head and neck squamous cell carcinoma [49]. However, both reports demonstrated that *ABCG2*-knockdown decreased cell migration and invasion in glioma stem cells by decreasing matrix metalloproteinase (MMP)-9 or MMP2/9 activity [50,51]. Nevertheless, our studies did not find significant difference in MMP-9 levels among four A549 stable cells (data not shown).

Collectively, these findings demonstrated that ABCG2 locates to the nucleus and binds to the *CDH1* promoter and then positively regulates E-cadherin expression in lung cancer cells. Additionally, ABCG2 could affect cell migration and tumor colonization *in vitro* and in the xenografted mouse model. Further analyses would be necessary to clarify the mechanism of ABCG2 shuttling among the membrane, cytosol, and nucleus. Changing the localization of ABCG2 from membrane to nucleus could be theoretically more effective for improving chemotherapy resistance and suppressing tumor cells with metastatic potential. Our results suggest that ABCG2 has dual functional activities, either as a transporter on the plasma membrane to exclude xenobiotics or as a transcriptional factor in the nucleus to regulate gene expressions, such as E-cadherin. It is interesting to note that the nuclear function of ABCG2 can contribute to modulation of tumor metastasis. Targeting ABCG2 as an anti-cancer treatment may thus be beneficial for the prevention of both drug resistance and/or cancer metastasis.

Supplementary data to this article can be found online at http://dx.doi.org/10.1016/j.neo.2015.01.004.

## Acknowledgements

The authors thank the Flow Cytometry Core Facility of the National Yang-Ming University and the National Microarray and Gene Expression Analysis Core Facility of the National Research Program for Genomic Medicine for providing technical services.

## References

[1] American Cancer Society (2013). Cancer Facts & Figures. Atlanta, GA: American Cancer Society; 2013 .

[2] Schinkel AH and Jonker JW (2003). Mammalian drug efflux transporters of the ATP binding cassette (ABC) family: an overview. *Adv Drug Deliv Rev* **55**, 3–29.

[3] Dean M (2009). ABC transporters, drug resistance, and cancer stem cells. *J Mammary Gland Biol Neoplasia* **14**, 3–9.

[4] Robey R, Polgar O, Deeken J, To K, and Bates S (2007). ABCG2: determining its relevance in clinical drug resistance. *Cancer Metastasis Rev* **26**, 39–57.

[5] Hirschmann-Jax C, Foster AE, Wulf GG, Nuchtern JG, Jax TW, Gobel U, Goodell MA, and Brenner MK (2004). A distinct "side population" of cells with high drug efflux capacity in human tumor cells. *Proc Natl Acad Sci U S A* **101**, 14228–14233.

[6] Ho MM, Ng AV, Lam S, and Hung JY (2007). Side population in human lung cancer cell lines and tumors is enriched with stem-like cancer cells. *Cancer Res* **67**, 4827–4833.

[7] Visvader JE and Lindeman GJ (2008). Cancer stem cells in solid tumours: accumulating evidence and unresolved questions. *Nat Rev Cancer* **8**, 755–768.

[8] Zhou S, Schuetz JD, Bunting KD, Colapietro AM, Sampath J, Morris JJ, Lagutina I, Grosveld GC, Osawa M, and Nakauchi H, et al (2001). The ABC transporter Bcrp1/ABCG2 is expressed in a wide variety of stem cells and is a molecular determinant of the side-population phenotype. *Nat Med* **7**, 1028–1034.

[9] Yoh K, Ishii G, Yokose T, Minegishi Y, Tsuta K, Goto K, Nishiwaki Y, Kodama T, Suga M, and Ochiai A (2004). Breast cancer resistance protein impacts clinical outcome in platinum-based chemotherapy for advanced non–small cell lung cancer. *Clin Cancer Res* **10**, 1691–1697.

[10] Ota S, Ishii G, Goto K, Kubota K, Kim YH, Kojika M, Murata Y, Yamazaki M, Nishiwaki Y, and Eguchi K, et al (2009). Immunohistochemical expression of BCRP and ERCC1 in biopsy specimen predicts survival in advanced non-small-cell lung cancer treated with cisplatin-based chemotherapy. *Lung Cancer* **64**, 98–104.

[11] Solazzo M, Fantappie O, D'Amico M, Sassoli C, Tani A, Cipriani G, Bogani C, Formigli L, and Mazzanti R (2009). Mitochondrial expression and functional activity of breast cancer resistance protein in different multiple drug-resistant cell lines. *Cancer Res* **69**, 7235–7242.

[12] Lemos C, Kathmann I, Giovannetti E, Dekker H, Scheffer GL, Calhau C, Jansen G, and Peters GJ (2008). Folate deprivation induces BCRP (ABCG2) expression and mitoxantrone resistance in Caco-2 cells. *Int J Cancer* **123**, 1712–1720.

[13] Chen JS, Pardo FS, Wang-Rodriguez J, Chu TS, Lopez JP, Aguilera J, Altuna X, Weisman RA, and Ongkeko WM (2006). EGFR regulates the side population in head and neck squamous cell carcinoma. *Laryngoscope* **116**, 401–406.

[14] Yeboah D, Kalabis GM, Sun M, Ou RC, Matthews SG, and Gibb W (2008). Expression and localisation of breast cancer resistance protein (BCRP) in human fetal membranes and decidua and the influence of labour at term. *Reprod Fertil Dev* **20**, 328–334.

[15] Bhatia P, Bernier M, Sanghvi M, Moaddel R, Schwarting R, Ramamoorthy A, and Wainer IW (2012). Breast cancer resistance protein (BCRP/ABCG2) localises to the nucleus in glioblastoma multiforme cells. *Xenobiotica* **42**, 748–755.

[16] Yang MH, Hsu DS, Wang HW, Wang HJ, Lan HY, Yang WH, Huang CH, Kao SY, Tzeng CH, and Tai SK, et al (2010). Bmi1 is essential in Twist1-induced epithelial-mesenchymal transition. *Nat Cell Biol* **12**, 982–992.

[17] Yang CY, Kuo TH, and Ting LP (2006). Human hepatitis B viral e antigen interacts with cellular interleukin-1 receptor accessory protein and triggers interleukin-1 response. *J Biol Chem* **281**, 34525–34536.

[18] Dennis Jr G, Sherman BT, Hosack DA, Yang J, Gao W, Lane HC, and Lempicki RA (2003). DAVID: Database for Annotation, Visualization, and Integrated Discovery. *Genome Biol* **4**, R60.1-60.11.

[19] Thiery JP and Sleeman JP (2006). Complex networks orchestrate epithelial-mesenchymal transitions. *Nat Rev Mol Cell Biol* **7**, 131–142.

[20] Huang WC, Chen YJ, Li LY, Wei YL, Hsu SC, Tsai SL, Chiu PC, Huang WP, Wang YN, and Chen CH, et al (2011). Nuclear translocation of epidermal growth factor receptor by Akt-dependent phosphorylation enhances breast cancer-resistant protein expression in gefitinib-resistant cells. *J Biol Chem* **286**, 20558–20568.

[21] Xie Y, Xu K, Linn DE, Yang X, Guo Z, Shimelis H, Nakanishi T, Ross DD, Chen H, and Fazli L, et al (2008). The 44-kDa Pim-1 kinase phosphorylates BCRP/ABCG2 and thereby promotes its multimerization and drug-resistant activity in human prostate cancer cells. *J Biol Chem* **283**, 3349–3356.

[22] Mogi M, Yang J, Lambert JF, Colvin GA, Shiojima I, Skurk C, Summer R, Fine A, Quesenberry PJ, and Walsh K (2003). Akt signaling regulates side population cell phenotype via Bcrp1 translocation. *J Biol Chem* **278**, 39068–39075.

[23] Bleau AM, Hambardzumyan D, Ozawa T, Fomchenko EI, Huse JT, Brennan CW, and Holland EC (2009). PTEN/PI3K/Akt pathway regulates the side population phenotype and ABCG2 activity in glioma tumor stem-like cells. *Cell Stem Cell* **4**, 226–235.

[24] Huang FF, Wu DS, Zhang L, Yu YH, Yuan XY, Li WJ, Chen XP, Zhao XL, Chen FP, and Zeng H (2013). Inactivation of PTEN increases ABCG2 expression and the side population through the PI3K/Akt pathway in adult acute leukemia. *Cancer Lett* **336**, 96–105.

[25] Baldini N, Scotlandi K, Serra M, Shikita T, Zini N, Ognibene A, Santi S, Ferracini R, and Maraldi NM (1995). Nuclear immunolocalization of P-glycoprotein in multidrug-resistant cell lines showing similar mechanisms of doxorubicin distribution. *Eur J Cell Biol* **68**, 226–239.

[26] Hennig G, Löwrick O, Birchmeier W, and Behrens J (1996). Mechanisms identified in the transcriptional control of epithelial gene expression. *J Biol Chem* **271**, 595–602.

[27] Hosono S, Gross I, English MA, Hajra KM, Fearon ER, and Licht JD (2000). E-cadherin is a WT1 target gene. *J Biol Chem* **275**, 10943–10953.

[28] Cano A, Perez-Moreno MA, Rodrigo I, Locascio A, Blanco MJ, del Barrio MG, Portillo F, and Nieto MA (2000). The transcription factor Snail controls epithelial-mesenchymal transitions by repressing E-cadherin expression. *Nat Cell Biol* **2**, 76–83.

[29] Batlle E, Sancho E, Franci C, Dominguez D, Monfar M, Baulida J, and Garcia de Herreros A (2000). The transcription factor Snail is a repressor of E-cadherin gene expression in epithelial tumour cells. *Nat Cell Biol* **2**, 84–89.

[30] Comijn J, Berx G, Vermassen P, Verschueren K, van Grunsven L, Bruyneel E, Mareel M, Huylebroeck D, and van Roy F (2001). The two-handed E box binding zinc finger protein SIP1 downregulates E-cadherin and induces invasion. *Mol Cell* **7**, 1267–1278.

[31] Hajra KM, Chen DY-S, and Fearon ER (2002). The SLUG zinc-finger protein represses E-cadherin in breast cancer. *Cancer Res* **62**, 1613–1618.

[32] Yang J, Mani SA, Donaher JL, Ramaswamy S, Itzykson RA, Come C, Savagner P, Gitelman I, Richardson A, and Weinberg RA (2004). Twist, a master regulator of morphogenesis, plays an essential role in tumor metastasis. *Cell* **117**, 927–939.

[33] Frixen UH, Behrens J, Sachs M, Eberle G, Voss B, Warda A, Löchner D, and Birchmeier W (1991). E-cadherin-mediated cell-cell adhesion prevents invasiveness of human carcinoma cells. *J Cell Biol* **113**, 173–185.

[34] Wendt MK, Taylor MA, Schiemann BJ, and Schiemann WP (2011). Down-regulation of epithelial cadherin is required to initiate metastatic outgrowth of breast cancer. *Mol Biol Cell* **22**, 2423–2435.

[35] Chao Y, Shepard C, and Wells A (2010). Breast carcinoma cells re-express E-cadherin during mesenchymal to epithelial reverting transition. *Mol Cancer* **9**, 1–18.

[36] Chaffer CL, Brennan JP, Slavin JL, Blick T, Thompson EW, and Williams ED (2006). Mesenchymal-to-epithelial transition facilitates bladder cancer metastasis: role of fibroblast growth factor receptor-2. *Cancer Res* **66**, 11271–11278.

[37] Dykxhoorn DM, Wu Y, Xie H, Yu F, Lal A, Petrocca F, Martinvalet D, Song E, Lim B, and Lieberman J (2009). miR-200 enhances mouse breast cancer cell colonization to form distant metastases. *PLoS One* **4**, 1–14 [e7181].

[38] Wu K, Fan J, Zhang L, Ning Z, Zeng J, Zhou J, Li L, Chen Y, Zhang T, and Wang X, et al (2012). PI3K/Akt to GSK3β/β-catenin signaling cascade coordinates cell colonization for bladder cancer bone metastasis through regulating ZEB1 transcription. *Cell Signal* **24**, 2273–2282.

[39] Stankic M, Pavlovic S, Chin Y, Brogi E, Padua D, Norton L, Massagué J, and Benezra R (2013). TGF-β-Id1 signaling opposes twist1 and promotes metastatic colonization via a mesenchymal-to-epithelial transition. *Cell Rep* **5**, 1228–1242.

[40] Kim M, Turnquist H, Jackson J, Sgagias M, Yan Y, Gong M, Dean M, Sharp JG, and Cowan K (2002). The multidrug resistance transporter ABCG2 (breast cancer resistance protein 1) effluxes Hoechst 33342 and is overexpressed in hematopoietic stem cells. *Clin Cancer Res* **8**, 22–28.

[41] Scharenberg CW, Harkey MA, and Torok-Storb B (2002). The ABCG2 transporter is an efficient Hoechst 33342 efflux pump and is preferentially expressed by immature human hematopoietic progenitors. *Blood* **99**, 507–512.

[42] Krishnamurthy P, Ross DD, Nakanishi T, Bailey-Dell K, Zhou S, Mercer KE, Sarkadi B, Sorrentino BP, and Schuetz JD (2004). The stem cell marker Bcrp/ABCG2 enhances hypoxic cell survival through interactions with heme. *J Biol Chem* **279**, 24218–24225.

[43] Korpal M, Ell BJ, Buffa FM, Ibrahim T, Blanco MA, Celia-Terrassa T, Mercatali L, Khan Z, Goodarzi H, and Hua Y, et al (2011). Direct targeting of Sec23a by miR-200s influences cancer cell secretome and promotes metastatic colonization. *Nat Med* **17**, 1101–1108.

[44] Celia-Terrassa T, Meca-Cortes O, Mateo F, de Paz AM, Rubio N, Arnal-Estape A, Ell BJ, Bermudo R, Diaz A, and Guerra-Rebollo M, et al (2012). Epithelial-mesenchymal transition can suppress major attributes of human epithelial tumor-initiating cells. *J Clin Invest* **122**, 1849–1868.

[45] Ocana OH, Corcoles R, Fabra A, Moreno-Bueno G, Acloque H, Vega S, Barrallo-Gimeno A, Cano A, and Nieto MA (2012). Metastatic colonization requires the repression of the epithelial-mesenchymal transition inducer Prrx1. *Cancer Cell* **22**, 709–724.

[46] Tsai JH, Donaher JL, Murphy DA, Chau S, and Yang J (2012). Spatiotemporal regulation of epithelial-mesenchymal transition is essential for squamous cell carcinoma metastasis. *Cancer Cell* **22**, 725–736.

[47] Li R, Liang J, Ni S, Zhou T, Qing X, Li H, He W, Chen J, Li F, and Zhuang Q, et al (2010). A mesenchymal-to-epithelial transition initiates and is required for the nuclear reprogramming of mouse fibroblasts. *Cell Stem Cell* **7**, 51–63.

[48] Samavarchi-Tehrani P, Golipour A, David L, Sung HK, Beyer TA, Datti A, Woltjen K, Nagy A, and Wrana JL (2010). Functional genomics reveals a BMP-driven mesenchymal-to-epithelial transition in the initiation of somatic cell reprogramming. *Cell Stem Cell* **7**, 64–77.

[49] Chang CC, Hsu WH, Wang CC, Chou CH, Kuo MY, Lin BR, Chen ST, Tai SK, Kuo ML, and Yang MH (2013). Connective tissue growth factor activates pluripotency genes and mesenchymal-epithelial transition in head and neck cancer cells. *Cancer Res* **73**, 4147–4157.

[50] Gong W, Wang Z, Wan Y, Shi L, and Zhou Y (2014). Downregulation of ABCG2 protein inhibits migration and invasion in U251 glioma stem cells. *Neuroreport* **25**, 625–632.

[51] Shi L, Wang Z, Sun G, Wan Y, Guo J, and Fu X (2014). miR-145 inhibits migration and invasion of glioma stem cells by targeting ABCG2. *Neuromolecular Med* **16**, 517–528.